Inorganic Chemistry

Article

pubs.acs.org/IC

Structural and Vibrational Properties of Silyl (SiH_3^-) Anions in $KSiH_3$ and $RbSiH_3$: New Insight into Si−H Interactions

Verina F. Kranak,[†] Yuan-Chih Lin,[‡] Maths Karlsson,[‡] Janos Mink,[§,∥] Stefan T. Norberg,[#] and Ulrich Häussermann*[,†]

[†]Department of Materials and Environmental Chemistry, Stockholm University, SE-10691 Stockholm, Sweden

[‡]Department of Applied Physics, Chalmers University of Technology, SE-41296 Gothenburg, Sweden

[§]Research Center of Natural Sciences, Hungarian Academy of Sciences, P.O. Box 77, H-1525, Budapest, Hungary

[∥]Research Institute of Chemical and Process Engineering, Faculty of Information Technology, University of Pannonia, P.O. Box 158, H-8201 Veszprém, Hungary

[#]Department of Chemical and Biological Engineering, Chalmers University of Technology, SE-41296 Gothenburg, Sweden

Supporting Information

ABSTRACT: The alkali metal silyl hydrides $ASiH_3$ (A = K, Rb) and their deuteride analogues were prepared from the Zintl phases ASi. The crystal structures of $ASiH_3$ consist of metal cations and pyramidal SiH_3^- ions. At room temperature SiH_3^- moieties are randomly oriented (α modifications). At temperatures below 200 K $ASiH_3$ exist as ordered low-temperature (β) modifications. Structural and vibrational properties of SiH_3^- in $ASiH_3$ were characterized by a combination of neutron total scattering experiments, infrared and Raman spectroscopy, as well as density functional theory calculations. In disordered α-$ASiH_3$ SiH_3^- ions relate closely to freely rotating moieties with C_{3v} symmetry (Si−H bond length = 1.52 Å; H−Si−H angle 92.2 °). Observed stretches and bends are at 1909/1903 cm^{-1} (ν_1, A_1), 1883/1872 cm^{-1} (ν_3, E), 988/986 cm^{-1} (ν_4, E), and 897/894 cm^{-1} (ν_2, A_1) for A = K/Rb. In ordered β-$ASiH_3$ silyl anions are slightly distorted with respect to their ideal C_{3v} symmetry. Compared to α-$ASiH_3$ the molar volume is by about 15% smaller and the Si−H stretching force constant is reduced by 4%. These peculiarities are attributed to reorientational dynamics of SiH_3^- anions in α-$ASiH_3$. Si−H stretching force constants for SiH_3^- moieties in various environments fall in a range from 1.9 to 2.05 N cm^{-1}. These values are considerably smaller compared to silane, SiH_4 (2.77 N cm^{-1}). The reason for the drastic reduction of bond strength in SiH_3^- remains to be explored.

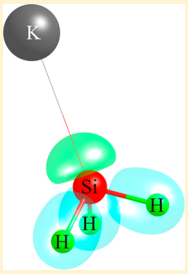

I. INTRODUCTION

Nucleophilic silyl anions SiR_3^- are important and versatile organometallic reagents which are employed in the synthesis of main group element clusters, compounds with elements in low oxidation states, and polysilanes with defined backbone geometries.[1] SiH_3^- is archetypal as the simplest silyl anion. Using various forms of spectroscopy and theoretical calculations the pyramidal ion has been frequently employed as a model system in fundamental investigations into structure, reactivity, and bonding properties of small molecules.[2−11]

Solutions of SiH_3^- can be prepared by reacting alkali metals (or their alloys) with silane, SiH_4, in polar aprotic solvents (e.g., monoglyme or diglyme). For A = K, Rb, and Cs the silyl hydrides $ASiH_3$ can be isolated solvent free and crystalline.[12−14] At room temperature crystalline $ASiH_3$ corresponds to a NaCl-type arrangement of alkali metal and Si atoms, meaning that pyramidal anions SiH_3^- are distributed in random orientations in the crystal structure (α-$ASiH_3$).[15,16] The nature of the disorder (dynamic, static, or mixed) has not yet been elucidated. At temperatures below 200 K $ASiH_3$ exist as hydrogen-ordered β modifications.[17−19]

Recently, it was shown that disordered α-$ASiH_3$ is also accessible by direct hydrogenation of the intermetallic compounds (or Zintl phases) ASi.[18,19] Compared to the solution-phase route, solid−gas reactions afford pure α-$ASiH_3$ after shorter reaction times and do not involve tedious solvent separation and purification steps. Further, hydrogenation of ASi to α-$ASiH_3$ is truly remarkable: Although silyl hydride formation is accompanied by a tremendous lattice expansion, the systems ASi/α-$ASiH_3$ show reversible H storage capability near ambient conditions. The advantageous thermodynamic characteristics of the sorption/desorption process is due to an unusually low entropy variation, which in turn has been attributed to the disorder in α-$ASiH_3$.[18] This finding added an interesting materials property aspect to silyl hydrides.

The origin and nature of the disorder in room-temperature α-$ASiH_3$ most likely relates to the peculiar coordination behavior of the SiH_3^- anion, which has already been described for molecular aggregates,[20,21] and eventually in its fundamental structure and bonding properties. It is then surprising that despite the obvious significance of SiH_3^- and its rather long history of examination these properties appear contradictory. The Si−H bond length has been reported as 1.47−1.49 Å in crystalline α-$ASiH_3$[18,19] and as around 1.54 Å for SiH_3^- anions in solution and from theoretical calculations.[4,6−9] Reported H−

Received: December 8, 2014
Published: February 10, 2015

DOI: 10.1021/ic502931e
Inorg. Chem. 2015, 54, 2300−2309

Si−H angles fluctuate between 92° and 95°.[3,6−9] Spectroscopy investigations of SiH_3^- and theoretical calculations of anharmonic frequencies yielded varying and sometimes contradictory results. For example, wavenumbers of the stretching fundamentals are scattered between 1800 and 1900 cm^{-1}.[4−8]

The aim of this work is to shed new light on the fundamental structure and bonding properties of SiH_3^- and correlate those to other prototypic silicon hydrides. In particular, by a combination of neutron total scattering experiments, optical spectroscopy, and first-principles calculations we show that the structural and vibrational properties of SiH_3^- in solid α- and β-$ASiH_3$ are different. In fact, we propose that SiH_3^- in disordered α-$ASiH_3$ relates closely to a freely rotating ion with vibrational properties very similar to a silyl ion in a polar solvent. Finally, we compare the vibrational and bonding properties of SiH_3^- with those of silane, SiH_4, and the hypervalent species SiH_6^{2-} and attempt to establish general trends associated with the Si−H bond. Although $CsSiH_3$ is known, we restricted our investigation to $KSiH_3$ and $RbSiH_3$.

II. EXPERIMENTAL AND CALCULATIONAL DETAILS

Synthesis. The silyl hydrides α-$KSiH_3$ and α-$RbSiH_3$ (α-$ASiH_3$) were synthesized according to refs 18 and 19. All steps of synthesis and sample preparation were performed in an Ar-filled glovebox (H_2O and O_2 levels < 0.1 ppm). The Zintl phases KSi and RbSi (*A*Si) were prepared from stoichiometric amounts of K (Aldrich, 99.9%), Rb (Aldrich, 99.9%), and Si (Chempur, crystalline powder, 99.999%). Si was pressed into pellets and placed alternately with the alkali metal in a tantalum ampule. The ampoules were heated inside a silica tube under vacuum at a rate of 5 K/min to 873 K, held for 30 h, and then cooled to room temperature at a rate of 5 K/min. α-$ASiH_3$ was obtained by heating pellets of KSi and RbSi in a corundum crucible in a stainless steel autoclave to 423 and 373 K, respectively, under a pressure of 50 bar of hydrogen for 24 h (H_2 AGA 99.99999%). The corresponding deuterides α-$ASiD_3$ were prepared accordingly (D_2 AGA 99.997%) but employing a longer reaction time (5 days). Hydride and deuteride samples were ground in an agate mortar for subsequent investigations.

Powder X-ray Diffraction (PXRD). PXRD patterns were recorded at room temperature on a Panalytical X'PERT PRO diffractometer employing either Cu Kα_1 or Cu Kα radiation. Due to the air and moisture sensitivity of all materials they were either sealed in 0.3 mm capillaries or mounted between two layers of Kapton tape in the glovebox. PXRD patterns of *A*Si were examined for phase purity. The diffraction patterns of cubic $ASiH_3$ and $ASiD_3$ were subjected to Rietveld analysis using the FullProf software.[22] Satisfactory fits required the refinement of the crystallite shape by a spherical harmonics expansion for the Laue class *m*-3*m*. The results of the refinement are shown in Figure S1, Supporting Information, and Table 1.

Neutron Scattering. Neutron powder diffraction data were obtained on the Polaris diffractometer at the ISIS pulsed spallation neutron source, Rutherford Appleton Laboratory, United Kingdom. Data were collected with the backscattering (130−160°), 90° (85−95°), low angle (28−42°), and very low angle (13−15°) detectors, providing a *Q* range of about 0.5−31 $Å^{-1}$. Samples were contained in cylindrical thin-walled 11 mm diameter vanadium cans which in turn were placed in a closed cycle cryostat, located in front of the backscattering detector. The measurement temperatures were 297 and 310 K for α-$RbSiD_3$ and α-$KSiD_3$, respectively. Data were collected for 1200 μA h to allow for total scattering analysis. Additionally, diffraction data from an empty vanadium can in the crystostat were collected for about 700 μA h to allow for data correction. The data were reduced and corrected for background scattering and beam attenuation employing the GudrunN software,[23] and the resulting normalized total scattering structure factors, $S(Q)$, were then used to obtain the corresponding pair distribution function, $D(r)$, via Fourier transformation.

Table 1. Structure Parameters for α-$ASiH_3$ (*A* = K, Rb) According to PXRD[a]

$Fm\bar{3}m$, $Z = 4$	α-$KSiH_3$	α-$KSiD_3$	α-$RbSiH_3$	α-$RbSiD_3$
a (Å)	7.2360(1)	7.2239(2)	7.50367(3)	7.49124(4)
V ($Å^3$)	378.87	376.98	422.49	420.40
B_{iso} *A*	4.89(17)	5.18 (13)	7.36(63)	5.37 (60)
B_{iso} Si	5.62 (21)	5.67 (16)	8.18(13)	5.45 (12)
d_{A-Si} (Å)	3.618	3.612	3.752	3.746
R_{wp}	13.1	11.8	5.71	11.3

[a]*A* atoms are situated on 4a (0,0,0) and Si atoms on 4b (0.5, 0.5, 0.5).

Spectroscopy. Mid-IR (350−4000 cm^{-1}, 128 scans, and resolution 4 cm^{-1}) absorption spectra were recorded by using a dynamically aligned Varian IR-670 spectrometer with a thermostatted DTGS detector. Spectra of samples were recorded with a "Golden Gate" micro-ATR accessory equipped with KRS-5 lenses and a diamond ATR element. Powdered samples of $ASiH_3$ and $ASiD_3$ were transferred from the glovebox in airtight vials. At the spectrometer the vials were opened and the powders were quickly clamped between the ATR diamond and sapphire elements. Obtained spectra did not show any evidence of sample decomposition (e.g., bands of O−H, Si−O). All IR spectra were ATR corrected.

For Raman spectroscopy powdered samples were sealed in 0.3 mm capillaries. Room-temperature spectra were measured using a Labram HR 800 spectrometer. The instrument is equipped with an 800 mm focal length spectrograph and an air-cooled (−70 °C), back-thinned CCD detector. Samples were excited using a double-frequency Nd:YAG laser (532 nm). Raman spectra were collected with an exposure time of 60 s and accumulation number of 10 and using a 600 grooves/mm grating. Low-temperature spectra (at 200 and 100 K) were measured with a Dilor XY-800 triple-grating spectrometer with double-subtractive configuration. This instrument is equipped with a liquid nitrogen-cooled CCD detector. Capillaries were placed in a Linkam temperature stage. A cooling rate of 3 K/min was applied, and the capillaries were equilibrated for 10 min after having reached the target temperature (i.e., 200 and 100 K). Samples were excited with a Ar^+/Kr^+ laser (647 nm). Data covering the spectral range 30−4000 cm^{-1} were collected in 18 spectral windows using a 1800 grooves/mm grating. The exposure time for each window was 120 s, and the number of accumulations was 10. Spectral windows were subsequently merged.

IR and Raman spectra were processed and evaluated with the GRAMS/AI (7.02) spectroscopy software suite.[24] Normal coordinate calculations were performed by means of the Wilson's **GF** matrix method. Force constants were obtained by optimizing the vibrational frequencies using a symmetrized valence force field. For the calculations the PC-based program package developed by J. Mink and L. Mink was used.[25]

Computation. Density functional theory (DFT) calculations were performed with the plane wave code Abinit[26] using the PBE parametrization for the exchange-correlation effects.[27] Norm-conserving pseudopotentials for Si and H were obtained from the fhi98PP package[28] of the Troullier-Martins scheme.[29] The norm-conserving pseudopotentials for K and Rb were set according to Goedecker, Teter, and Hutter.[30] These potentials are optimized for use with PBE. The crystal structures of β-$ASiH_3$ were relaxed with respect to volume, lattice parameters, and atomic positions. Forces were converged to better than 10^{-3} eV/Å. The integration over the Brillouin zone (BZ) was performed on special Monkhorst−Pack *k*-point grids.[31] The kinetic energy cutoffs were set at 375 eV (β-$ASiH_3$). Maximally localized Wannier functions,[32] phonon dispersion relations, and zero-point energy (ZPE) corrected structures were calculated with respect to the relaxed equilibrium structures.

DOI: 10.1021/ic502931e
Inorg. Chem. 2015, 54, 2300−2309

III. RESULTS AND DISCUSSION

Crystal Structures of α- and β-$ASiH_3$ (A = K, Rb). The hydrogenation of RbSi and KSi at 373 and 423 K, respectively, affords roentgenographically pure samples of α-$ASiH_3/D_3$ with an average cubic NaCl-type structure in which SiH_3^- units are disordered. Table 1 lists the structural parameters of our materials. PXRD patterns are given in the Supporting Information (Figure S1). The unit cell parameters are in excellent agreement with those reported previously for α-$ASiH_3/D_3$.[18,19]

Chotard et al.[18] and Tang et al.[19] refined the structure of α-$ASiD_3$ from neutron powder diffraction data with a model where D atoms were distributed on a weakly occupied (12%) Wyckoff site 96k in the $Fm\bar{3}m$ NaCl structure. In this model Si is regularly ("spherically") surrounded by 24 D atom positions (occupied at a 12% level) at a distance of 1.47 and 1.48 Å for A = K and Rb, respectively. The simple model provides a very reasonable crystallographic description of the disorder in which pyramidal SiH_3^- ions are randomly aligned along the four body diagonals (i.e., the C_3 axes) of the cubic unit cell. In addition, each body diagonal direction allows for an "up" and a "down" alignment. Thus, the average crystallographic structure of disordered $ASiH_3$ is based on eight (random) orientations for each SiH_3^- ion. The model, of course, does not address the nature of the disorder (static vs dynamic), which still remains unclear. Also, Rietveld analysis, as applied in refs 18 and 19, is not able to probe local structure aspects of the disorder and may have limitations when it comes to reliably refining the positional parameters of the very weakly occupied D atom site.

The study of local structure features in disordered α-$ASiD_3$ requires the analysis of total scattering data.[33] While such an analysis will be described elsewhere, we present here the pair distribution function (PDF), $D(r)$, of α-$KSiD_3$ and α-$RbSiD_3$ extracted from neutron total scattering data (Figure 1). The

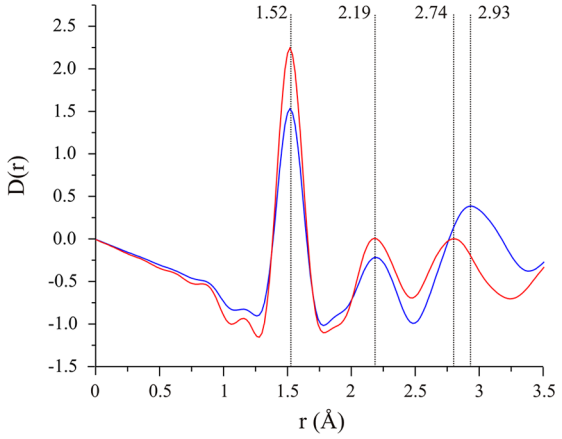

Figure 1. Pair distribution functions $D(r)$ for α-$KSiD_3$ (red) and α-$RbSiD_3$ (blue) extracted from neutron total scattering data. Location of maxima correspond to the interatomic pairs Si−D, D−D, A−D. Distances are indicated in Angstroms.

positions of the peaks in a PDF correspond to the separation of pairs of atoms. The PDFs of α-$ASiD_3$ display three distinct and sharp peaks for the region r < 3.5 Å, whereas peaks for r > 3.5 Å are very broad as a consequence of the disorder (not shown in Figure 1). For both A = K, Rb the first two peaks have their maxima exactly at the same positions, r = 1.52 and 2.19 Å. These peaks correspond to the Si−D and D−D distances in the silyl anion. Therefore we can conclude that the geometry of SiD_3^- is identical in both compounds and that the D−Si−D angle is 92.2°. The third peak in the PDFs refers to the A−D distance, which is at 2.74 and 2.93 Å for A = K and Rb, respectively. Thus, from a simple inspection of the PDF the geometry of the silyl anion in disordered α-$ASiD_3$ can be unambiguously deduced. The Si−D distance is significantly larger compared to the one obtained from Rietveld refinement (1.52 vs 1.47 Å).

Below 200 K crystalline $ASiH_3$ exist in low-temperature (β) forms.[16,17] It should be emphasized that the α-to-β transition is accompanied with a drastic reduction of the molar volume (by about 15%) for all systems. Recently, Tang et al. established fully the structures of hydrogen ordered β-$ASiH_3$ from neutron powder diffraction experiments (on β-$ASiD_3$).[19] β-$KSiH_3$ crystallizes with the orthorhombic space group $Pnma$. Silyl groups possess a local C_s symmetry, which implies two different Si−H distances and H−Si−H bond angles (Figure 2a). The β

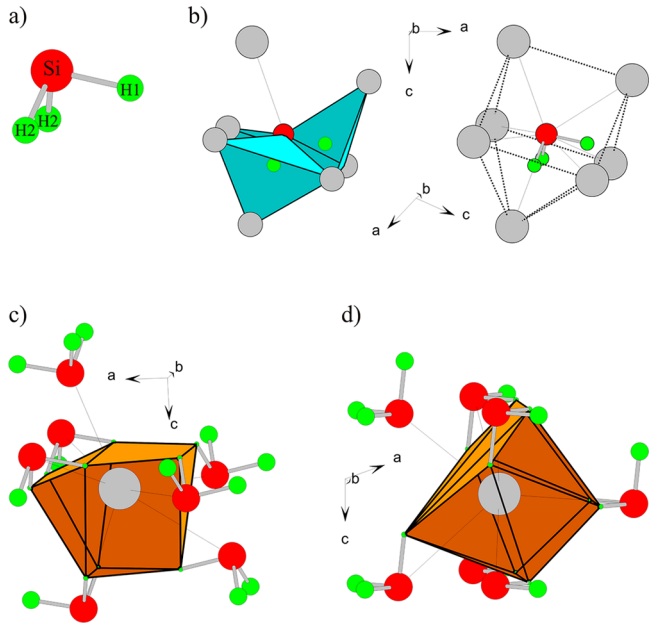

Figure 2. Structural features of β-$ASiH_3$. Green, red, and gray circles denote H, Si, and A atoms, respectively. (a) Silyl anion with C_s symmetry possessing one short (Si−H1) and two long (Si−H2) distances. (b) Coordination environment of the Si atoms. (Left) Three H ligands are coordinated by three A^+ ions each. Resulting $HSiA_3$ tetrahedra (cyan) share edges. (Right) The seventh A^+ ion coordinates the lone pair of Si. The coordination polyhedron of A^+ around a SiH_3^- moiety corresponds to a monocapped trigonal prism. (c) Coordination environment of the A^+ ions in orthorhombic β-$KSiH_3$ (left) and monoclinic β-$RbSiH_3$ (right). Orange polyhedra indicate the nearest neighbor coordination by 9 H atoms stemming from six silyl groups. A seventh silyl ion is coordinated via the Si lone pair.

modifications of $RbSiH_3$ and $CsSiH_3$ adopt the monoclinic $P2_1/m$ $KClO_3$ structure. The crystal symmetry lowering does not affect the local symmetry of the silyl anions and their coordination by countercations. This coordination is shown in Figure 2b. Each H ligand is coordinated by three A^+ ions, which results in a quasi-tetrahedral environment. H coordination involves 6 A^+ ions around a Si atom; the three $HSiA_3$ tetrahedra share common edges. The seventh A^+ ion around a Si atom is situated on the pseudo-3-fold axis of the anion, coordinating its "lone pair" site. This is usually referred to as "tetrahedral

DOI: 10.1021/ic502931e
Inorg. Chem. 2015, 54, 2300−2309

coordination" for molecular systems.[20,21] The polyhedron defined by the 7 A^+ cations encapsulating SiH_3^- corresponds to a monocapped trigonal prism, which can be considered as a common building block of both the orthorhombic and the monoclinic β structures.[19] In the two structures monocapped trigonal prisms are linked differently. As a consequence, the coordination of A^+ by silyl groups is different (Figure 2c and 2d).

The geometrical parameters of the SiD_3^- anion in β-$KSiD_3$ and β-$RbSiD_3$ are compiled in Table 2. The experimental data

Table 2. Geometry of SiD_3^-/SiH_3^- Ions in β-$ASiH_3/D_3$.

	$KSiD_3$ exp.[a]	$KSiH_3$ DFT (ZPE)	$RbSiD_3$ exp.[a]	$RbSiH_3$ DFT
Si–D1 (Å)	1.537(8)	1.543 (1.542)	1.496(13)	1.544
Si–D2 (Å) × 2	1.545(6)	1.556 (1.555)	1.546(8)	1.555
$(Si–D)_{av}$ (Å)	1.542	1.551 (1.551)	1.529	1.551
D2–Si–D2 (deg)	93.8(1)	92.2 (92.4)	91.4(1)	92.3
D2–Si–D1 (deg) × 2	93.9(1)	93.0 (93.2)	93.7(1)	93.0
$(D2–Si–D1)_{av}$ (deg)	93.9	92.7 (92.9)	92.9	92.8

[a]Data from Tang et al.[18]

from Tang et al. (measured at 1.5 K)[18] are compared to our DFT optimizations (referring to β-$ASiH_3$). Characteristically, the C_s silyl anions have one "short" Si–H1/D1 and two "long" Si–H2/D2 distances and one "small" and two "large" bond angles. The DFT-optimized structures suggest that the geometry of the silyl anion is virtually identical in both systems. The distortion from the ideal C_{3v} symmetry is small: Short and long Si–H distances differ by about 0.012 Å, and the two bond angles differ by about 0.75°. Importantly, the geometry of the silyl anion is not affected when considering ZPE (only tested for β-$KSiH_3$). In the experimental crystal structures of β-$ASiD_3$ the geometry of SiD_3^- deviates slightly. The difference between the short and the long Si–D distance is 0.008 and 0.020 Å for A = K and Rb, respectively. Bond angles are somewhat larger and their splitting less pronounced for A = K.

We also discuss the average geometry of the silyl anion in β-$ASiH_3/D_3$. According to the DFT calculations the average Si–H bond length and H–Si–H bond angle are 1.55 Å and 92.8°, respectively, for both systems. Experimental Si–D bond lengths (D–Si–D angles) at 1.5 K are 1.54 and 1.53 Å (93.9° and 92.9°) for A = K and Rb, respectively.[19] The PDFs from neutron scattering data obtained at 200 K reveal a Si–D bond length of 1.54 Å for both systems (Supporting Information, Figure S3). We note that, despite some spread of the data, the average geometry of SiD_3^- in β-$ASiD_3$ should correspond closely to the one in disordered α-$ASiD_3$. However, the bond length and angle are slightly smaller in the latter (1.52 Å and 92.2°). This observation will be important for the interpretation of the spectroscopic properties of ordered and disordered $ASiH_3$. H/D isotope effects may explain the small difference between DFT-calculated Si–H and the experimentally determined Si–D distance (at 1.5 K). However, this is not clear, and we do not consider isotope effects as significant for the bond length in SiH_3/D_3^-.

Spectroscopy on α-$ASiH_3$. Raman and IR (ATR) spectra of α-$ASiH_3/D_3$ were measured at room temperature. The spectra of α-$ASiH_3$ are displayed in Figure 3. For a pyramidal

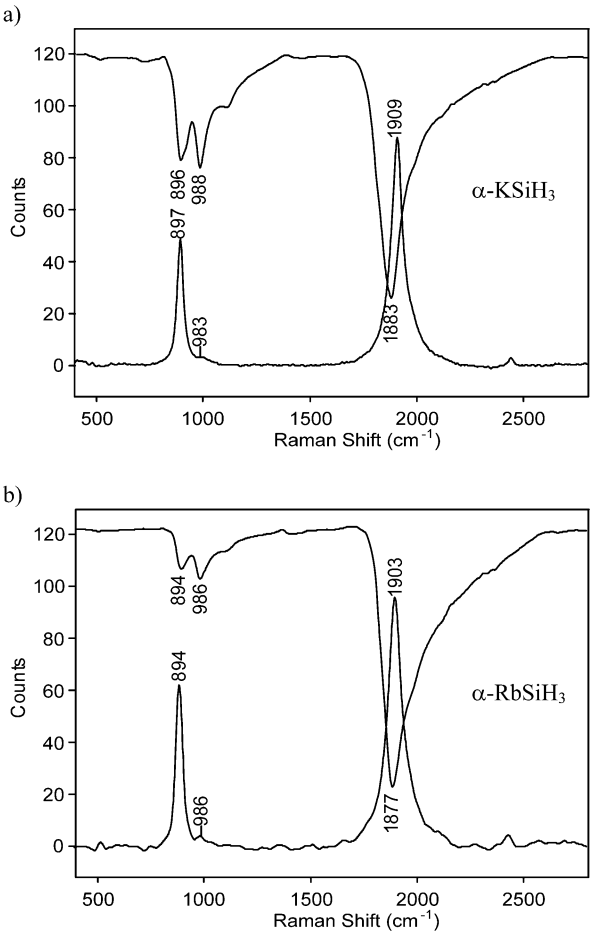

Figure 3. Comparison of the infrared (ATR) (upper trace) and Raman (lower trace) spectra of α-$KSiH_3$ (a) and α-$RbSiH_3$ (b) recorded at room temperature in the spectral range of the fundamental vibrations of the SiH_3^- anion. Spectra were normalized to the most intensive lines as 100 relative intensity units. IR trace is an absorbance spectrum multiplied by −1.

SiH_3^- anion with C_{3v} symmetry one expects two symmetric (A_1) and two asymmetric (E) vibrations. The four vibrations are both IR and Raman active. The spectra of α-$ASiH_3/D_3$ contain only bands that are associated with these vibrations (internal modes). Lattice (external) modes, which are associated with libration (torsion) of SiH_3^- moieties and translation of A^+ and SiH_3^- ions, are absent. IR bands are at around 1880, 987, and 895 cm^{-1}, and strong Raman bands are at around 1905 and 895 cm^{-1}. The Raman bands are broad but display a highly symmetric shape.[34] This is similar for high-temperature spectra of alkali metal borohydrides[35,36] and suggests the presence of reorientationally disordered silyl anions.

The location and assignment of bands for α-$ASiH_3/D_3$ are compiled in Table 3. Tables summarizing a complete evaluation of spectra are supplied as Supporting Information (Table S1 (hydrides) and Table S2 (deuterides)). The assignment of X–H stretching modes may be problematic for pyramidal C_{3v} species when bond angles H–X–H become close to 90°. For example, PH_3 and SH_3^+, which are isoelectronic to SiH_3^-, display bands where the asymmetric (ν_3) and symmetric (ν_1) modes are very close and even overlapping.[37,38] In the spectra of α-$KSiH_3$ we assign the strong Raman band at 1909 cm^{-1} and the strong IR band at 1883 cm^{-1} to the symmetric and

DOI: 10.1021/ic502931e
Inorg. Chem. 2015, 54, 2300–2309

Table 3. Experimental and Calculated Fundamental Modes (cm^{-1}) for SiH_3^- and SiD_3^- Anions with C_{3v} Symmetry in $ASiH_3D_3$

exp.	calcd[a]	exp.	calcd[a]	assignments
$KSiH_3$		$KSiD_3$		
1909	1910	1381	1380	ν_1, A_1 symmetric SiH/SiD stretch
897	898	654	652	ν_2, A_1 symmetric SiH/SiD bend
1883	1884	1359	1358	ν_3, E asymmetric SiH/SiD stretch
988	989	709	705	ν_4, E asymmetric SiH/SiD bend
$RbSiH_3$		$RbSiD_3$		
1903	1907	1381	1378	ν_1, A_1 symmetric SiH/SiD stretch
894	896	654	650	ν_2, A_1 symmetric SiH/SiD bend
1877	1881	1358	1356	ν_3, E asymmetric SiH/SiD stretch
986	990	708	706	ν_4, E asymmetric SiH/SiD bend

[a]From force constant calculations (see Discussion in text) using a H−Si−H bond angle of 92.2° and a Si−H distance of 1.52 Å.

asymmetric Si−H stretching mode of SiH_3^-, respectively. The assignment $\nu_1 > \nu_3$ is supported by measurements of $KSiH_3$ in solution[4] and from theoretical calculations of SiH_3^-,[6−8] although reported wavenumbers are quite different from ours, which will be discussed at a later stage. The location of the stretching bands is virtually identical for α-$RbSiH_3$. These bands are shifted for the deuterides to the region 1360−1380 cm^{-1}. The isotope shift is around 1.38 (cf. Table 3).

The double-degenerate bending mode (ν_4) appears as a strong IR band at 988 cm^{-1} and is at higher energies than the umbrella vibration (ν_2), which is seen at 897 cm^{-1} as a strong Raman feature. The relationship $\nu_4 > \nu_2$ is valid for all investigated systems. These bands are shifted to the region 660−710 cm^{-1} for SiD_3^-. Finally, weak overtones and combination bands could be detected in the IR spectra. They are assigned in Tables S1 and S2 (Supporting Information).

We conclude that the spectra of NaCl-type α-$ASiH_3$ can be interpreted solely on the basis of the internal vibrations of silyl ions possessing C_{3v} symmetry. The countercation (viz. K^+ or Rb^+) has virtually no influence on the location of the bands. Bands could be unambiguously assigned to the fundamentals ν_1−ν_4. We note that the stretching frequencies observed by us represent the highest hitherto reported for SiH_3^- from an experiment. Force constants were calculated and refined on the basis of the measured fundamental frequencies. The Si−H stretching force constant was obtained as 2.038 and 2.032 N cm^{-1} for A = K and Rb, respectively. Details of the force constant calculations are given as Supporting Information, Table S3. The stretch−stretch interaction terms for SiH_3^- anions are small (about 0.011 N cm^{-1}), indicating a very weak coupling between vibrating Si−H bonds. Therefore, the individual Si−H bond stretches behave as so-called "local" modes (independent oscillators), which is a common behavior for molecules with symmetrically equivalent X−H bonds.[39] Fundamental frequencies calculated with the refined force constants are included in Table 3.

Spectroscopy on β-$ASiH_3$. Raman spectra of β-$ASiH_3/D_3$ were measured at 200 and 100 K. In the following the 100 K spectra of β-$ASiH_3$ are discussed. The orthorhombic and monoclinic unit cells of β-$KSiH_3$ and β-$RbSiH_3$ contain four and two formula units, respectively. Hence, there are 24 and 12 internal mode vibrations, respectively. According to factor group analysis[40,41] the internal modes distribute as $4A_g + 2B_{1g} + 4B_{2g} + 2B_{3g} + 2A_u + 4B_{1u} + 2B_{2u} + 4B_{3u}$ for the orthorhombic ($Pnma$) case and as $4A_g + 2B_g + 2A_u + 4B_u$ for the monoclinic ($P2_1/m$) case. The "g" modes are Raman active vibrations, one-half each account for stretches and bends. In contrast with the room-temperature spectra, the low-temperature ones clearly show bands of external (lattice) modes which are located below 500 cm^{-1} (Figures S2a and S2c, Supporting Information). This part of the spectrum is of minor importance to the bonding properties of the silyl anion. Therefore, we do not address it here.

Figure 4 compares the spectra of α/β-$KSiH_3$ and α/β-$RbSiH_3$ in the spectral range of the internal modes (800−2000 cm^{-1}). Broad bands in the room-temperature spectra become narrow and distinct lines at low temperature. In particular, the bands of the asymmetric modes, which are barely discernible in the spectra of the α forms, are clearly visible in the low-temperature spectra. In addition, the asymmetric (E) modes are split into A′ and A″ components as a consequence of the symmetry lowering of the SiH_3^- anion from C_{3v} to C_s. For β-$KSiH_3$ the two components of the asymmetric stretch ν_2 are at

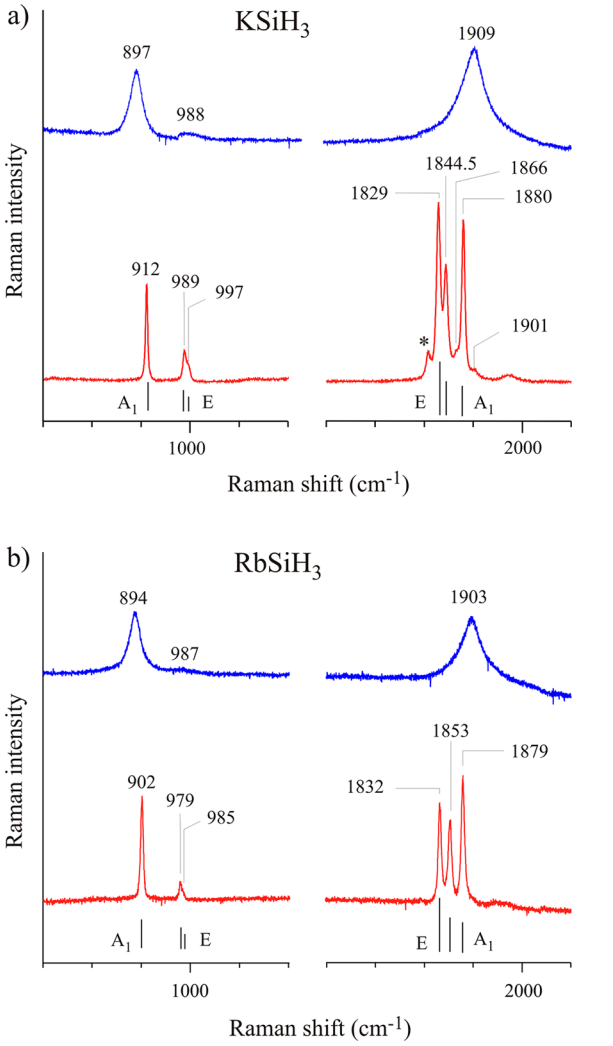

Figure 4. Comparison of Raman spectra of α-$ASiH_3$ (room temperature, upper trace) and β-$ASiH_3$ (100 K, lower trace) in the spectral range of the internal modes: (a) A = K and (b) A = Rb. Wavenumbers of the bands are inset (in cm^{-1}). Asterisk marks a band corresponding to an overtone or combination band of lattice modes or their combination with internal modes. This band is absent in the spectrum of β-$KSiD_3$ (Figure S2b, Supporting Information).

DOI: 10.1021/ic502931e
Inorg. Chem. 2015, 54, 2300−2309

1844 and 1829 cm^{-1} and the ones for the asymmetric bend ν_4 at 997 and 989 cm^{-1}.

In the ordered β-forms silyl anions possess one short and two long bonds (cf. Table 2). The established "local" mode behavior of stretches suggests strongly that different bond lengths should express themselves with different force constants (i.e., one "large" and two "small" Si−H stretching force constants). In Tables 4 and 5 experimentally observed bands for β-$ASiH_3$ are matched to the ones obtained from force constant calculations. These force constants are compiled in Table 6 and discussed later. There is good agreement with the experimental Raman bands. The difference in the stretching force constant associated with the short and long bond is 0.09−0.1 N cm^{-1}. This difference accounts for the size of the observed splittings, which is on the order of 15−20 cm^{-1} for the stretches and 6−8 cm^{-1} for the bends.

Table 4. Assignment of Raman Bands (cm^{-1}) of β-$KSiH_3$ (at 100 K) Accounting for the Internal Modes of the SiH_3^- Anion

exp.[a]	calcd[b]	calcd[c]	assignment (*Pnma*)
1901 (100)	1884 (A′)	1901	B_{2g} out-of-phase symmetric stretch
1880 (1670)		1866	A_g in-phase symmetric stretch
1866 (360)			
1844.5 (1200)	1843 (A′)	1849	B_{2g} out-of-phase asymmetric stretch
		1838	A_g in-phase asymmetric stretch
1829 (1850)	1837 (A″)	1823	B_{1g} in-phase asymmetric stretch
		1822	B_{3g} out-of-phase asymmetric stretch
997 (150)	1003 (A′)	960	B_{2g} out-of-phase asymmetric bend
		957	A_g in-phase asymmetric bend
989 (320)	995 (A″)	950	B_{3g} out-of-phase asymmetric bend
		947	B_{1g} in-phase asymmetric stretch
912 (960)	914 (A′)	885	B_{2g} out-of-phase umbrella mode
		879	A_g in-phase umbrella mode

[a]Relative Raman line intensities are in brackets (counts). [b]Force constant calculation. Single molecular unit calculation with different Si−H bond lengths (1.543 and 1.556 Å (2×)) and H−Si−H bond angles (93.0° and 92.2° 2×)). For details see text. [c]DFT calculation.

Table 5. Assignment of Raman Bands (cm^{-1}) of β-$RbSiH_3$ (at 100 K) Accounting for the Internal Modes of the SiH_3^- Anion

exp.[a]	calcd[b]	calcd[c]	assignment ($P2_1/m$)
1879 (1600)	1882 (A′)	1908	A_g symmetric stretch
1853 (1200)	1845.5 (A′)	1882	A_g asymmetric stretch
1832 (1300)	1837 (A″)	1857	B_g asymmetric stretch
985 (150)	1001 (A′)	998	A_g asymmetric bend
979 (200)	999.5 (A″)	993	B_g asymmetric bend
902 (1300)	912 (A′)	930	A_g umbrella mode (symmetric bend)

[a]Relative Raman line intensities are in brackets (counts). [b]Force constant calculation. Single molecular unit calculation with different Si−H bond lengths (1.543 and 1.556 Å (2 ×)) and H−Si−H bond angles (93.0 and 92.2° 2 ×)). For details see text. [c]DFT calculation.

For orthorhombic β-$KSiH_3$ the six Raman frequencies should then be split further into two components each when considering the interaction (vibrational coupling) between SiH_3^- units in the crystal (correlation splitting).[40,41] This adds up to the total number of possible Raman active ("g") modes. Tables 4 and 5 contain also wavenumbers of Raman active modes from DFT calculations. The DFT-calculated correlation splitting ranges from 1 to 12 cm^{-1} for ν_2−ν_4-derived modes. It is even 35 cm^{-1} for the symmetric Si−H stretching vibrations (ν_1) for which modes are calculated at 1901 (B_{2g}) and 1866 cm^{-1} (A_g). However, only one well-defined band is observed at 1880 cm^{-1}; two weaker features are at 1901 and 1866 cm^{-1} (cf. Figure 3, Table 4). The strongest band should be assigned to the A_g mode. The weak band at 1901 cm^{-1} may then be the B_{2g} vibration, whereas the weak band at 1866 cm^{-1} remains unassigned. However, we rather conclude that it is not possible to detect correlation splitting in the experimental spectra (see also the spectra of the deuterides, Figures S2b and S2d, Supporting Information). When averaging correlation splitting, the DFT-calculated wavenumbers of stretches agree very well (within 1%) with experiment. In contrast, bending modes are somewhat underestimated (by about 6%). For β-$RbSiH_3$ DFT-calculated wavenumbers of both stretches and bends are slightly overestimated (between 1% and 3%).

Comparison of the Silyl Anion in Different Environments. Our study aimed at the spectroscopic characterization of the silyl anion in solid $ASiH_3$, whereas earlier investigations concerned SiH_3^- in the gas phase and in solution. Table 6 summarizes our results and previous ones.

We first compare ordered β-$ASiH_3$ and disordered α-$ASiH_3$ and note an appreciable difference in the Si−H stretching force constant. The value for C_s SiH_3^- (~1.956 N cm^{-1}, from averaging the large and small force constants) is by 4% lower than the value for C_{3v} SiH_3^- (~2.035 N cm^{-1}). The strengthening of the Si−H bond in the disordered room-temperature phase appears surprising. There are many complex hydrides (e.g., alanates, borohydrides, Mg_2NiH_4) displaying temperature-induced order−disorder transitions.[42,43] In fact, in

Table 6. Evaluation of Internal Modes (cm^{-1}) and Geometry for SiH_3^-

			$KSiH_3$		$RbSiH_3$		
gas phase[a]	He matrix[b]	solution phase[c]	300 K (C_{3v})	100 K (C_s)	300 K (C_{3v})	100 K (C_s)	description
1841	1856	1905[g]	1909 vs (R)	1880 vs	1903 vs (R)	1879 vs	ν_1 (A_1), symmetric stretch (cm^{-1})
1821	1837	1880 vs (IR)	1883 vs (IR)	1844 vs 1829 vs	1877 vs (IR)	1853 s 1832 s	ν_3 (E), asymmetric stretch (cm^{-1})[d]
938	930[g]	1000[g]	988 vs (IR)	997 w, sh 989 m	986 vs (IR)	979 w, sh 985 m	ν_4 (E), asymmetric bend (cm^{-1})[d]
844	850[g]	862 vs (R)	897 s (R)	912 vs	894 s (R)	902 s	ν_2 (A_1), symmetric bend (cm^{-1})[e]
1.901	1.936	2.03[g]	2.038	2.014, 1.925 × 2	2.032	2.028, 1.922 × 2	Si−H stretching force constants (N cm^{-1})[f]
1.538	1.54[g]	1.54[g]	1.52	1.543, 1.556 × 2^h	1.52	1.544, 1.555 × 2^h	Si−H bond lengths (Å)
95.2	95.2[g]	95.2[g]	92.2	92.2, 93 × 2^h	92.2	92.2 93, × 2^h	H−Si−H bond angles (deg)

[a]CCSD(T)-R12 level calculations by Aarset et al.[8] [b]Data from Andrews et al.[6] [c]Data from Bürger et al.[4,5] [d]Degenerate (E) modes in C_{3v} are split into A′ and A″ modes in C_s symmetry. [e]The umbrella mode obtained from photoelectron spectra is at 880 cm^{-1}.[3] [f]For details on force constant calculations, see Supporting Information Tables S3−S5. [g]Estimated. [h]According to DFT-optimized β-$ASiH_3$ structures, cf. Table 2.

DOI: 10.1021/ic502931e
Inorg. Chem. 2015, 54, 2300−2309

this respect the silyl hydrides $ASiH_3$ relate well to the heavier alkali metal borohydrides ABH_4 (A = Na–Cs) for which the disordered high-temperature forms also adopt a NaCl-type average structure.[35] We are not aware that the phenomenon of bond strength increase has been reported for the order–disorder transitions in ABH_4.

We also note that the large molar volume difference between α- and β-$ASiH_3$ (about 15%) is unparalleled among complex hydride systems. Typically, molar volume changes associated with order–disorder transitions are around 5%. We make the conjecture that α-$ASiH_3$ represents a rotator phase, that is, silyl anions correspond to quasi freely rotating moieties (through rotational and reorientational jumps), which are confined within the octahedral cavity of six A^+ cations in the NaCl-type structure. Clearly, the molar volume has to be considerably lower for rigidly coordinated silyl anions, and the Si–H bond could strengthen significantly upon release of a rigid A–H coordination. Strong evidence of pronounced dynamics comes from the drastic widening of Raman lines when going from the ordered to the disordered phase. The HWHM of the symmetric stretch (ν_1) is about 100 cm^{-1}, and that of the symmetric bend (ν_2) is around 50 cm^{-1}. Dynamic disorder will also explain that the bands of the less intense asymmetric (E) modes are barely noticeable in the Raman spectra of α-$ASiH_3$ (cf. Figures 3 and 4). A conclusive elucidation of the dynamic disorder in α-$ASiH_3$, however, will require quasielastic neutron scattering and/or NMR investigations.

We now turn to C_{3v} SiH_3^- as a gas-phase species. There are no experimental investigations of gaseous SiH_3^-, but we consider the results of the quartic force field calculation by Aarset et al. applying a nearly converged basis set and treatment of correlation as an accurate description of gaseous SiH_3^-.[8] These authors obtained the values 1841, 844, 1821, and 938 cm^{-1} for the fundamentals ν_1, ν_2, ν_3, and ν_4. These values are very low compared to C_{3v} SiH_3^- in solid α-$ASiH_3$. Accordingly, the Si–H stretching force constant is considerably reduced (1.901 vs 2.035 N cm^{-1}). Furthermore, the geometry of the gas-phase species (1.538 Å and 95.2°) is rather different than the C_{3v} ion in α-$ASiH_3$ (1.52 Å and 92.2°). It should be emphasized here that these geometries are ascertained from the high-quality calculation and the neutron PDFs, respectively. Consequently, well-defined force fields can be established. Using these force fields as a reference, we investigated the variations of the ν_1–ν_4 fundamentals upon changing the H–Si–H bond angle in the experimentally relevant range between 90° and 96° (see Supporting Information for details). The result is shown in Figure 5. It is seen (i) that especially the bending modes (ν_2, ν_4) are highly susceptible to bond angle changes, (ii) that the pairs ν_1 and ν_2 (A_1 symmetry) and ν_3 and ν_4 (E symmetry) change in a parallel way, and (iii) that absolute changes (as seen in the slopes) are virtually the same for C_{3v} SiH_3^- in the gas phase and in solid α-$ASiH_3$. Importantly, for C_{3v} SiH_3^- in the solid (stiffer force field) the splitting of the stretches ν_1 and ν_3 is smaller and that of the bends ν_2 and ν_4 is larger compared to the gas-phase species. The bond angle variation relations will prove useful when interpreting the properties of SiH_3^- in different environments.

The substantially increased wavenumbers (and stiffer force constant) for SiH_3^- in α-$ASiH_3$ as compared to the gas phase are attributed to the A^+ environment (blue shift or hypsochromic shift). Concomitantly, but not necessarily related, there is a decrease in bond length and angle. This suggests that the—presumably quasi freely rotating—C_{3v} silyl

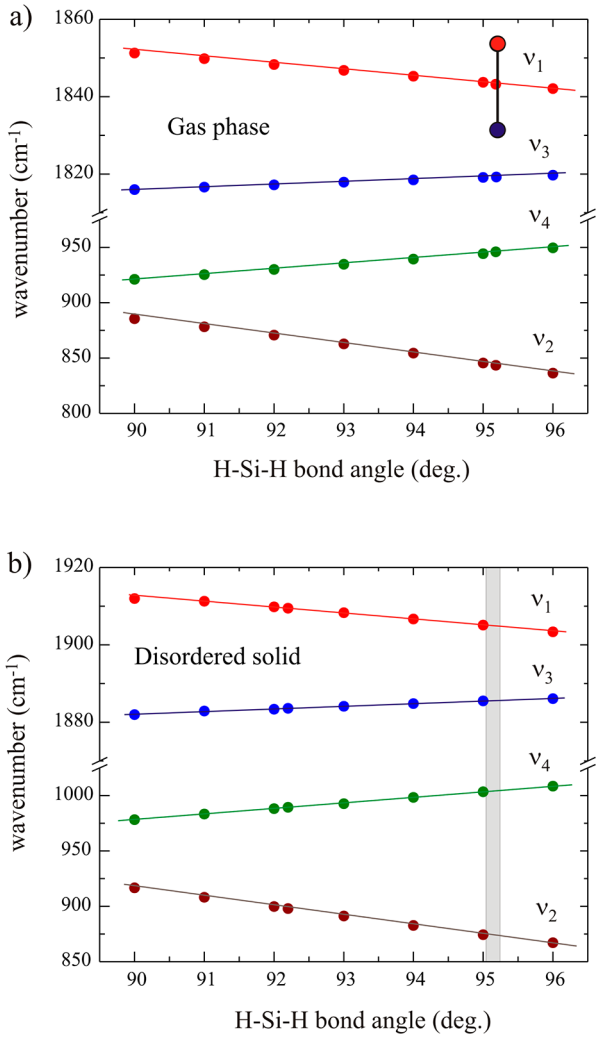

Figure 5. Variation of the wavenumber of C_{3v} SiH_3^- fundamentals as a function of the H–Si–H bond angle. (a) Using a force field reflecting the gas-phase species. The vertical bar marks the difference between ν_1 and ν_3 for the He matrix-isolated species (according to ref 6). (b) Using a force field reflecting the disordered species in α-$KSiH_3$. Gray area marks the situation of SiH_3^- ions in polar aprotic solvents (according to ref 4). For details, see Supporting Information.

ions encaged in A^+ octahedra in the α-$ASiH_3$ structure appear compressed with respect to the gas-phase species. The average geometry of C_s SiH_3^- in β-$ASiH_3$ relates closer to the gas-phase species. Also, the Si–H stretching force constant falls in between that of C_{3v} SiH_3^- in α-$ASiH_3$ and the gas-phase species. Naturally, closest agreement with the gas-phase species is then seen for the He matrix species, as analyzed by Andrews and Wang.[6] Although these authors reported only two stretching frequencies (ν_1 and ν_3 at 1856 and 1837 cm^{-1}, respectively) we can use the difference to estimate the bond angle from the relations shown in Figure 5. As expected, the value corresponds to that of the gas-phase species (95.2°). The missing frequencies (ν_2 and ν_4) as well as the force constant can now be estimated and are included in Table 6. The slightly larger force constant compared to the gas-phase species reflects the interaction of the He matrix with SiH_3^-.

Finally, we turn to SiH_3^- in solution. The investigation by Bürger et al. yielded only two reliably determined wavenumbers, ν_2 and ν_3.[4,5] Their difference is 1018 cm^{-1} which,

DOI: 10.1021/ic502931e
Inorg. Chem. 2015, 54, 2300–2309

with the correlations established in Figure 5, allows the conclusion that (i) a polar aprotic solvent environment induces a similar blue shift (with respect to the gas-phase species) as the octahedral A^+ environment in α-$ASiH_3$ and (ii) the bond angle of SiH_3^- in solution is similar to the gas-phase species (~95°). Again, one can now estimate the missing frequencies (ν_1 and ν_4) and the Si−H stretching force constant. The latter is very similar to SiH_3^- in solid α-$ASiH_3$ (2.03 N cm^{-1}).

This comparative analysis shows that the vibrational properties of the silyl anion are highly susceptible to the environment, i.e., stretching fundamentals may differ by up to 70 cm^{-1}. Interestingly, a polar solvent and the cation environment in solid α-$ASiH_3$ have a comparable "interaction strength" toward SiH_3^-. The silyl ion has a very similar geometry in solution, as matrix-isolated species and in the gas phase (referring to the quasi converged theoretical calculation), Si−H ≈ 1.54 Å and H−Si−H ≈ 95 °. In the solid state the bond angle is decreased. In the high-temperature form, in addition, the bond length is reduced.

Correlating Si−H Bonds. After having firmly established the vibrational properties of the SiH_3^- ion we turn to a comparison with other silicon hydride species. For example, how does SiH_3^- relate to prototypic SiH_4 and SiH_6^{2-}? The former exemplifies a system with a strong Si−H bond (Si−H bond length 1.47 Å). The recently reported hypervalent complex SiH_6^{2-} in K_2SiH_6 has a very weak Si−H bond (Si−H bond length 1.62 Å).[44] We attempted to establish a general correlation of Si−H stretching force constants and Si−H bond lengths in silicon hydrides (see Supporting Information for details on the force constant calculations, Tables S6−S9, Supporting Information).[45] This is shown in Figure 6 where stretching force constants are plotted for various species $SiH_n^{\nu\pm}$ (n = 1−6) against $(r)^{-1/3}$, thus investigating a Badger-type relation.[46,47] Although the limited number of $SiH_n^{\nu\pm}$ species (n = 1−4, 6) does not provide sound conclusions based on statistics, a roughly linear correlation may be assumed. The inset of Figure 6 highlights the various SiH_3^- species.

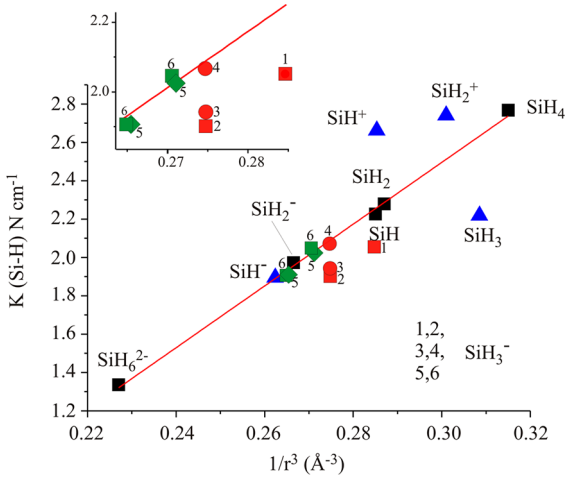

Figure 6. Plot of stretching force constants against the inverse cube of the Si−H bond length for various $SiH_n^{\nu\pm}$ species: (1) α-$ASiH_3$ (this work), (2) SiH_3^- gas-phase species (according to ref 8), (3) SiH_3^- matrix-isolated species (according to ref 6), (4) SiH_3^- in solution (according to ref 4), (5) β-$KSiH_3$ (long and short Si−H distance, this work), (6) β-$RbSiH_3$ (long and short Si−H distance, this work); (black squares) data from experiments, (blue triangles) data from theoretical calculations. (Inset) Situation of SiH_3^- species.

On the basis of this plot one may divide $SiH_n^{\nu\pm}$ species into three groups: (i) normal valent where Si does not carry a lone electron pair, e.g., SiH_4, force constants > 2.4 N cm^{-1}; (ii) normal valent where Si carries a lone pair (i.e., the oxidation state of Si is either +I or +II), e.g., SiH_3^-, singlet SiH_2, SiH, SiH^+, SiH^-, SiH_2^-, force constant 1.8−2.3 N cm^{-1}; (iii) hypervalent, e.g., SiH_6^{2-}, SiH_5^-, force constant < 1.5 N cm^{-1}. Although rare, hypervalent silyl hydride species extend considerably the range of Si−H interactions. Si−H stretching force constants can span from ~1.35 to ~2.7 N cm^{-1}. Among main group elements only B−H and Al−H interactions show a similar range of relative bond strength variation.

The substantial weakening of the Si−H bond when going from normal valent neutral to charged, lone pair carrying species was already noticed by Bürger et al.[4,5] Although this phenomenon appears fundamental, we are not aware of an explanation. One may compare with the pairs CH_4/CH_3^-, NH_3/NH_2^-, and PH_3/PH_2^- and it is noticed also here a decrease of stretching mode frequencies.[48−50] However, the relative change is considerably smaller than what is observed for SiH_4/SiH_3^-. Important perhaps is to consider that, compared to C−H, N−H, and P−H, the Si−H moiety is hydridic, that is, the polarity of the bond is reversed. At the same time, the small difference in electronegativity suggests that the bond polarity is rather weak (silicon 1.8, hydrogen 2.1). With respect to direction and magnitude of bond polarity, SiH_3^- should relate well to BH_4^-.

The occupied bands in the electronic band structure of β-$KSiH_3$ mirror the MO levels of a C_{3v} SiH_3^- ion (Figure 7a).

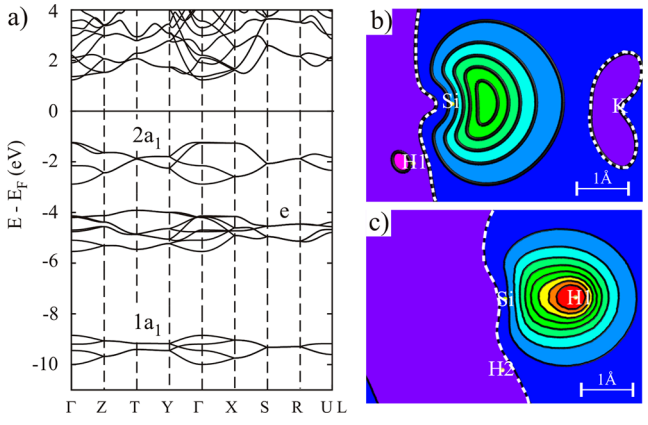

Figure 7. (a) Band structure for β-$KSiH_3$ at the computationally relaxed equilibrium volume. The Fermi level is indicated by a horizontal line and set at the center of the band gap. Bands are labeled with respect to the MOs of C_{3v} SiH_3^-. Contour maps for MLWFs associated with the lone electron pair (b) and the Si−H1 bond (c) in β-$KSiH_3$. Contours correspond to same values; the broken white lines separate positive from negative values.

The 1a_1- and e$_1$-type bands are Si−H bonding; the 2a_1-type bands centered at around −2 eV below the Fermi level are nonbonding. The DFT-calculated band gap is about 3 eV. The maximally localized Wannier functions (MLWFs) for β-$KSiH_3$ are shown in Figure 7b and 7c. They essentially reproduce the expected bonding picture of SiH_3^- with one Si−H1 and two Si−H2 bond orbitals (which are virtually indistinguishable) and one MLWF accounting for the nonbonding orbital. The shape of the latter suggests a substantial Si p-orbital contribution. The presence of a (sterochemically active) lone pair at Si was expected from the coordination geometry of the silyl anion in

DOI: 10.1021/ic502931e
Inorg. Chem. 2015, 54, 2300−2309

the β-$ASiH_3$ structures (cf. Figure 2b). The combination of a lone pair with hydridic hydrogen ligands is a peculiar feature of the silyl anion. Wolstenholme et al. have shown that for molecular systems "tetrahedral" (lone pair) and "inverted" (H_3) coordination of SiH_3^- by K^+ are essentially energetically degenerate.[21] Accordingly, pyramidal SiH_3^- can act as an ambidentate ligand. It is interesting to speculate whether the dynamic properties of SiH_3^- in α-$ASiH_3$ are a manifestation of this ambidentate behavior

IV. CONCLUSIONS

Neutron total scattering experiments, optical spectroscopy, as well as DFT calculations were employed to gain deeper insights into the structural and vibrational properties of the silyl anion SiH_3^- in the hydrides $ASiH_3$ (A = K, Rb), which have been recently identified as near ambient hydrogen storage systems. The findings are summarized as follows.

(1) Structural and vibrational properties of SiH_3^- in low-temperature β-$ASiH_3$ and room-temperature α-$ASiH_3$ are slightly but distinctly different. These differences are attributed to dynamically disordered SiH_3^- in α-$ASiH_3$. The vibrational properties of SiH_3^- in α-$ASiH_3$ relate well to those of silyl anions in polar aprotic solvents. Its structural properties correspond to that of a slightly compressed gas-phase species (Si−H bond length = 1.52 Å; H−Si−H angle 92.2°). The detailed nature of the dynamics of SiH_3^- in α-$ASiH_3$—and its relation to hydrogen storage properties—needs to be established from QENS and/or NMR experiments.

(2) Compared to silane, SiH_4, the Si−H stretching force constant for SiH_3^- is reduced by about 25%. The reason for the drastic weakening of the Si−H bond is not clear and deserves further investigations by theorists. Formally both SiH_4 and SiH_3^- are normal valent moieties with classical 2c2e Si−H bonds. The simple bonding picture can also be extracted from electronic structure calculations. SiH_3^- possesses a stereochemically active lone pair. The combination of a lone pair and hydridic H ligands is believed to be the origin of the ambidentate coordination behavior of the SiH_3^- ion. Dynamic disorder of SiH_3^- in α-$ASiH_3$ could be an expression of this ambidendate behavior.

■ ASSOCIATED CONTENT

Supporting Information

PXRD patterns of α-$KSiH_3$, α-$KSiD_3$, α-$RbSiH_3$, α-$RbSiD_3$; Raman spectra of β-$KSiH_3$, β-$KSiD_3$, β-$RbSiH_3$, β-$RbSiD_3$; PDFs of α-$KSiD_3$ and α-RbSiD3 at 200 K; observed IR and Raman bands for α-$KSiH_3$ and α-$RbSiH_3$; observed IR and Raman bands for α-$KSiD_3$ and α-$RbSiD_3$; details on force constant calculations and force constants for SiH_3^- in α-$KSiH_3$ and α-$RbSiH_3$; comparison of refined force constants for α- and β-$ASiH_3$; comparison of experimental and calculated fundamental frequencies for SiH_3^- and SiD_3^- anions in β-$ASiH_3$ and β-$ASiD_3$; force constants for SiH_4 and SiH_6^{2-}; experimental and calculated fundamental vibrations for SiH_4 and SiD_4; experimental and calculated fundamental frequencies for SiH_6^{2-}; stretching force constants for other $SiH_n^{\nu\pm}$ species. This material is available free of charge via the Internet at http://pubs.acs.org.

■ AUTHOR INFORMATION

Corresponding Author

*E-mail: Ulrich.Haussermann@mmk.su.se.

Notes

The authors declare no competing financial interest.

■ ACKNOWLEDGMENTS

This work was supported by the U.S. National Science Foundation (NSF-DMR-1007557) and the Swedish Research Council (2010-4827). We gratefully acknowledge the Science and Technology Facilities Council (STFC) for neutron beam time at the ISIS Facility, Rutherford Appleton Laboratory, and Drs. R. Smith and M. G. Tucker for assistance in performing the measurements and extracting PDF data. Finally, we are grateful to an anonymous reviewer for highly valuable comments.

■ REFERENCES

(1) Lerner, H.-W. *Coord. Chem. Rev.* **2005**, *249*, 781−798.
(2) Reed, K. J.; Brauman, J. I. *J. Chem. Phys.* **1974**, *61*, 4830−4838.
(3) Nimlos, M. R.; Ellison, G. B. *J. Am. Chem. Soc.* **1986**, *108*, 6522−6529.
(4) Bürger, H.; Eujen, R. *Z. Naturforsch. B* **1974**, *29*, 647−653.
(5) Bürger, H.; Eujen, R.; Marsmann, H. C. *Z. Naturforsch. B* **1974**, *29*, 149−152.
(6) Andrews, L.; Wang, X. *J. Phys. Chem. A* **2002**, *106*, 7696−7702.
(7) Shen, M.; Schaefer, H. F., III *Mol. Phys.* **1992**, *76*, 467−474.
(8) Aarset, K.; Csaszar, A. G.; Sibert, E. L., III; Allen, W. D.; Schaefer, H. F., III; Klopper, W.; Noga, J. *J. Chem. Phys.* **2000**, *112*, 4053−4063.
(9) Pak, C.; Rienstra-Kiracofe, J. C.; Schaefer, H. F., III *J. Phys. Chem. A* **2000**, *104*, 11232−11242.
(10) Sheldon, J. C.; Bowie, J. H.; DuPuy, C. H.; Damrauer, R. *J. Am. Chem. Soc.* **1986**, *108*, 6794−6800.
(11) DePuy, C. H.; Damrauer, R; Bowie, J. H.; Sheldon, J. C. *Acc. Chem. Res.* **1987**, *20*, 127−133.
(12) Ring, M. A.; Ritter, D. M. *J. Am. Chem. Soc.* **1961**, *83*, 802−805.
(13) Amberger, E.; Römer, R.; Layer, A. J. *Organomet. Chem.* **1968**, *12*, 417−423.
(14) (a) Feher, F.; Betzen, G.; Krancher, M. *Z. Anorg. Allg. Chem.* **1981**, *475*, 81−86. (b) Feher, F.; Krancher, M. *Z. Anorg. Allg. Chem.* **1984**, *509*, 95−100.
(15) Ring, M. A.; Ritter, D. M. *J. Am. Chem. Soc.* **1961**, *65*, 182−183.
(16) Weiss, E.; Hencken, G.; Kuhr, H. *Chem. Ber.* **1970**, *103*, 2868−2872.
(17) Mundt, O.; Becker, G.; Hartmann, H.-M.; Schwarz, W. *Z. Anorg. Allg. Chem.* **1989**, *572*, 75−88.
(18) Tang, W. S.; Chotard, J.-N.; Raybaud, P.; Janot, R. *J. Phys. Chem. C* **2014**, *118*, 3409−3419.
(19) Chotard, J.-N.; Tang, W. S.; Raybaud, P.; Janot, R. *Chem. Eur. J.* **2011**, *17*, 12302−12309.
(20) Flock, M.; Marschner, C. *Chem. Eur. J.* **2005**, *11*, 4635−4642.
(21) Wolstenholme, D. J.; Prince, P. D.; McGrady, G. S.; Landry, M. J.; Steed, J. W. *Inorg. Chem.* **2011**, *50*, 11222−11227.
(22) Rodríguez-Carvajal, J. *Physica B* **1993**, *192*, 55−69.
(23) Soper, A. Gudrun is a suite of programs with a graphic interface for the full correction of neutron diffraction data from various instruments at ISIS pulsed spallation neutron source; http://www.isis.stfc.ac.uk/groups/disordered-materials/.
(24) *GRAMS/AI 7.02*; Thermo Informatics: Madison, WI, 2002.
(25) Mink, J.; Mink, L. *Computer program system for vibrational analysis of polyatomic molecules (in Lahey-Fujitsu Fortran Win32)*; Stockholm, 2004.
(26) Gonze, X.; et al. *Comput. Phys. Commun.* **2009**, *180*, 2582−2615.
(27) Perdew, J. P.; Burke, K.; Ernzerhof, M. *Phys. Rev. Lett.* **1996**, *77*, 3865−3868.
(28) Fuchs, M.; Scheffler, M. *Comput. Phys. Commun.* **1999**, *119*, 67−98.

DOI: 10.1021/ic502931e
Inorg. Chem. 2015, 54, 2300−2309

(29) Troullier, N.; Martins, J. L. *Phys. Rev. B* **1991**, *43*, 1993.
(30) (a) Goedecker, S.; Teter, M.; Hutter, J. *Phys. Rev. B* **1996**, *54*, 1703. (b) Hartwigsen, C.; Goedecker, S.; Hutter, J. *Phys. Rev. B* **1998**, *58*, 3641. (c) Krack, M. *Theor. Chem. Acc.* **2005**, *114*, 145.
(31) (a) Monkhorst, H. J.; Pack, J. D. *Phys. Rev. B* **1976**, *13*, 5188−5192. Blöchl, P. E.; Jepsen, O.; Andersen, O. K. *Phys. Rev. B* **1994**, *49*, 16223−16234.
(32) (a) Marzari, N.; Vanderbilt, D. *Phys. Rev. B.* **1997**, *56*, 12847−12865. (b) Mostofi, A. A.; Yates, J. R.; Lee, Y.-S.; Souza, I. *Comput. Phys. Commun.* **2008**, *178*, 685−699. (c) Souza, I.; Marzari, N.; Vanderbilt, D. *Phys. Rev. B.* **2002**, *65*, 035109.
(33) (a) Egami, T.; Billinge, S. J. L. *Underneath the Bragg peaks: structural analysis of complex materials*; Pergamon Press Elsevier: Oxford, England, 2003, p 14. (b) Billinge, S. J. L.; Levin, I. *Science* **2007**, *316*, 561−565.
(34) The IR bands have an asymmetric component which is attributed to specular reflectance features, possibly due to a high refractive index of α-$ASiH_3$.
(35) Renaudin, G.; Gomes, S.; Hagemann, H.; Keller, L.; Yvon, K. *J. Alloys Compd.* **2004**, *375*, 98−106.
(36) Hagemann, H.; Gomes, S.; Renaudin, G.; Yvon, K. *J. Alloys Compd.* **2004**, *363*, 126−129.
(37) Sennikov, P. G.; Raldugin, D. A.; Nabiev, S. S.; Revin, V. A.; Khodzhiev, B. S. *Spectrochim. Acta, A* **1996**, *52*, 453−463.
(38) Xia, C. H..; Sanz, M. M.; Foster, S. C. *J. Mol. Spectrosc.* **1998**, *188*, 175−181.
(39) Baggott, J. E.; Clase, H. J.; Mills, I. M. *Spectrochim. Acta, A* **1986**, *42*, 319−334.
(40) Schrader, B. *Infrared and Raman Spectroscopy, Methods and Applications*; WCH: Weinheim, 1995.
(41) Nakamoto, K. *Infrared and Raman spectra of Inorganic and Coordination Compounds, Part A*, 6th ed.; John Wiley & Sons: New York, 2009.
(42) Jain, I. P.; Jain, P.; Jain, A. J. *Alloys Compd.* **2010**, *503*, 303−339.
(43) (a) Yvon, K.; Schefer, J.; Stucki, F. *Inorg. Chem.* **1981**, *20*, 2776−2778. (b) Zolliker, P.; Yvon, K.; Jorgensen, J. D.; Rotella, F. J. *Inorg. Chem.* **1986**, *25*, 3590−3593.
(44) Puhakainen, K.; Benson, D.; Nylen, J.; Konar, S.; Stoyanov, E.; Leinenweber, K.; Haussermann, U. *Angew. Chem., Int. Ed.* **2012**, *51*, 3156−3160.
(45) Experimental stretching frequencies and bond lengths were collected from the following. (a) Allen, W. D.; Schaefer, H. F., III *Chem. Phys.* **1986**, *108*, 243−274 and references therein. (b) Herzberg, G. *Molecular Spectra and Molecular Structure, I. Spectra of Diatomic Molecules*, 2nd ed.; van Nostrand: Toronto, New York, London, 1950. *Infrared and Raman spectra of polyatomic molecules*; van Nostrand: New York, 1945; pp 215−218. (c) Carlson, T. A.; Copley, J.; Duri, N.; Elander, N.; Erman, P.; Larsson, M.; Lyra, M. *Astron. Astrophys.* **1980**, *83*, 238−244. (d) Hirota, E.; Ishikawa, H. J. *Chem. Phys.* **1999**, *110*, 4254−4257. (e) Andrews, L.; Wang, X. *J. Phys. Chem. A* **2002**, *106*, 7696−7702. (f) Davies, P. B.; Isaacs, N. A.; Johnson, S. A.; Russell, D. K. *J. Chem. Phys.* **1985**, *83*, 2060−2063.
(46) (a) Badger, R. M. *J. Chem. Phys.* **1934**, *2*, 128−131. (b) Badger, R. M. *J. Chem. Phys.* **1935**, *3*, 710−714. (c) Herschbach, D. R.; Laurie, V. W. *J. Chem. Phys.* **1965**, *35*, 458−463.
(47) Kraka, E.; Larsson, J. A.; Cremer, D. Generalization of the Badger rule based on the use of adiabatic vibrational modes. In *Computational Spectroscopy: Methods, Experiments and Applications*; Grunenberg, J., Ed.; Wiley-VCH: Weinheim, 2010; pp 105−149.
(48) Weiss, E.; Sauermann, G.; Thirase, G. *Chem Ber.* **1983**, *116*, 74−85. (b) Weiss, E.; Corbelin, S.; Cockcroft, J. K.; Firch, A. N. *Chem. Ber.* **1990**, *123*, 1629−1634.
(49) Linde, G.; Juza, R. *Z. Anorg. Allg. Chem.* **1974**, *409*, 199−214.
(50) Jacobs, H.; Hassiepen, K. M. *Z. Anorg. Allg. Chem.* **1985**, *531*, 108−118.

DOI: 10.1021/ic502931e
Inorg. Chem. 2015, 54, 2300−2309